

Journal homepage: http://www.journalijar.com

INTERNATIONAL JOURNAL OF ADVANCED RESEARCH

### RESEARCH ARTICLE

## Electronic spectra, and DFT calculations of some triazolo [1,5-a]pyrimidine derivatives

Mohamed E. Elshakre, \*Hussein Moustafa, Huwaida M. E. Hassaneen, Khaled Saad Abdullah. Chemistry Department, Faculty of Science, Cairo University, Giza, EGYPT

Manuscript Info	Abstract
Manuscript History:	Ground state properties of 5,7-diphenyl-4,7-dihydro-[1,2,4]triazolo[1,5-a]pyrimidine, compound <b>1</b> , and its derivatives are investigated
Received: 14 March 2015 Final Accepted: 18 April 2015 Published Online: May 2015	experimentally and theoretically in 1,4-Dioxane (Dioxane) and N,N-Dimethylformamide (DMF). The calculations show that all the studied compounds 1-7 are non-planar as indicated from the values of the dihedral
Key words:	angles, resulting in a significant impact on the electronic and structural properties. The ground state properties of compounds 1-7 at B3LYP/6-
Triazolo[1,5-a]pyrimidine,UV, DFT/B3LYP, TD-DFT, solvent effect.	311G(df,pd) show that compound <b>2</b> ,which contains the nitro group, has the lowest $E_{LUMO}$ and $E_g$ , indicating highest reactivity. Compound <b>7</b> is found to have the highest polarity. The observed UV spectra in Dioxane and DMF of
*Corresponding Author	compounds 1, 2, 4, 5 and 6 exhibit 2 bands in both solvents, compound 3 exhibits 4 bands in Dioxane and 3 bands in DMF, while compound 7 exhibits 3 bands in both solvents. The difference in the spectral features of the studied
Hussein Moustafa	compounds can be attributed to the extent of the hyper conjugation of the triazolo[1,5-a]pyrimidine moiety and the nature of the substituent of the two phenyl groups. Band maxima ( $\lambda_{max}$ ) and intensities of the spectra are found to have solvent dependence reflected as blue and red shifts. The theoretical spectra computed at TD-B3LYP/6-311G(d,p) in gas phase, Dioxane and DMF nicely reproduce the observed spectra.

Copy Right, IJAR, 2015,. All rights reserved

### INTRODUCTION

Triazolopyrimidine derivatives are fused heterocyclic derivatives that have a broad range of activities. It was found that some of these compounds have analgesic, anticonvulsant, anti-inflammatory [1], antimicrobial [2], growth inhibition of some microorganisms [3], antitumor [4-8], antiparasitics [9], inhibition of p. falciparum [10], anticancer agents [11-14], antibiotic agent [15], adsorption inhibitors for the corrosion of mild steel [16], inhibition of the CD40 Pathway of Monocyte Activation [17], antifungal [18], macrophage activation [19], hepatitis C virus polymerase inhibitors [20], acetohydroxyacid synthase inhibitor [21], potential agents against trypanosomatids [22], antibacterial agents [23-25], adenosine A<sub>2a</sub> receptor antagonists [26, 27], latent leishmanicidal [28], antimalarial [29], human adenosine  $A_3$  receptor ligands [30], cardiovascular vasodilators [31], and herbicides activities [32]. Intense studies and calculations have been obtained for triazolopyrimidine derivatives, where the UV spectra of some triazolopyrimidine derivatives were studied, the results show the effect of the polar and non-polar solvents on the intensities and  $\lambda_{max}$  of the peaks observed in the UV spectra [33], Moxon et al obtained the absorption and fluorescence spectra of one triazolopyrimidine compound in a wide range of solvents [34], for triazolopyrimidine complexes, UV-Vis spectroscopies of copper(II), nickel(II) and zinc(II) complexes were investigated [35]. Furthermore, a ruthenium(II) complex binding with a triazolopyrimidine ligand was prepared and experimentally studied by UV-Vis spectroscopy, where its electronic structure and UV-Vis spectrum were calculated using the TD-DFT method [36]. Dobado et al [37] performed molecular orbital studies on anionic and neutral structures of

some triazolopyrimidine derivatives at B3LYP/6-311+G\*\* level and the quality of the theoretical results has been tested against the experimental X-ray structures for the three most stable neutral forms, yielding very good agreement. A more recent molecular orbital study was performed on different compounds of triazolopyrimidine derivatives at DFT-B3LYP/6-31G level of theory and excited states were calculated using ZINDO/S [33].

The UV spectroscopic studies along with HOMO–LUMO analysis have been used to elucidate information regarding charge transfer within the molecule. One key approach to understand solvent effects is the solvent-induced changes in the electronic transition of solutes, generally referred to as solvatochromism. Because of the wide range of biological activities of the triazolopyrimidine derivatives, these proposed triazolo [1,5-a] pyrimidine derivatives are considered of scientific interest to be explored. The electronic structures of molecules usually manifest itself in the electronic absorption and emission spectra, this manifestation enables the detailed understanding of the forces that govern the electronic structure of the studied triazolo [1, 5-a] pyrimidine derivatives.

Although, several investigations have been published that dealt with the electronic spectra of some triazolopyrimidine derivatives, yet there is no such systematic study of solvent and substituent effect on the observed spectra for these proposed triazolo [1,5-a] pyrimidine derivatives, such study is of critical importance in understanding their electronic structure which may correlate with their biological activity. The aim of this work is: (1) to explore the ground state properties of the studied triazolo [1,5-a] pyrimidine derivatives at the Density Functional level of Theory (DFT) method using B3LYP/6 -311G(df, pd); (2) study the type and extent of conjugative interaction between different subsystems of triazolo [1,5-a] pyrimidine derivatives; (3) the effect of solvent polarity on the observed spectra by using Dioxane as a nonpolar solvent and DMF as a polar solvent. These two solvents were selectively chosen because of their excellent dissolving ability of the studied sold compounds, hence, predicting the relative stabilities, extent of charge transfer character and assignment of the observed electronic transitions; (4) the effect of different substituents on the electronic spectra of triazolo [1,5-a] pyrimidine derivatives.

# 2. Experimental

### 2.1 Compounds

The compounds studied were prepared and purified using standard procedures cited in the literature [38]. The proposed molecules consist of two fused triazolopyrimidine rings attached to two terminal phenyl groups via pyrimidine ring. Substituent effect is investigated by insertion of various substituents in position 4 in both phenyl groups, Ph-X and Ph-Y, as shown in scheme 1, which shows the structure of the seven proposed compounds **1-7** of triazolo [1, 5-a] pyrimidine derivatives, where compound **1** is 5,7-diphenyl-4,7-dihydro-[1,2,4] triazolo [1,5-a] pyrimidine, **2** is 5-(4-fluorophenyl)-7-(4-nitrophenyl)-4,7-dihydro-[1,2,4] triazolo [1,5-a] pyrimidine, **3** is 5-(4-fluorophenyl)-4,7-dihydro-[1,2,4] triazolo [1,5-a] pyrimidine, **5** is 7-(4-bromophenyl)-5-(4-fluorophenyl)-4,7-dihydro-[1,2,4] triazolo [1,5-a] pyrimidine, **7** is 7-(4-fluorophenyl)-5-(4-methoxyphenyl)-4,7-dihydro-[1,2,4] triazolo [1,5-a] pyrimidine, **7** is 7-(4-fluorophenyl)-5-(4-methoxyphenyl)-4,7-dihydro-[1,2,4] triazolo [1,5-a] pyrimidine.

Triazolopyrimidine Compounds	X	Y
1	Н	Н
2	$NO_2$	F

3	OCH <sub>3</sub>	F
4	F	F
5	Br	F
6	CH <sub>3</sub>	F
7	F	OCH <sub>3</sub>

Scheme 1

#### 2.2 Solvents

Polar (Dimethyl Formamide, DMF) and non-polar (Dioxane) were obtained from Merck, AR grade and used without further purification. The two solvents show excellent dissolving ability for compound 5,7-diphenyl-4,7-dihydro-[1,2,4] triazolo [1,5-a] pyrimidine and its derivatives.

### 2.3 Apparatus

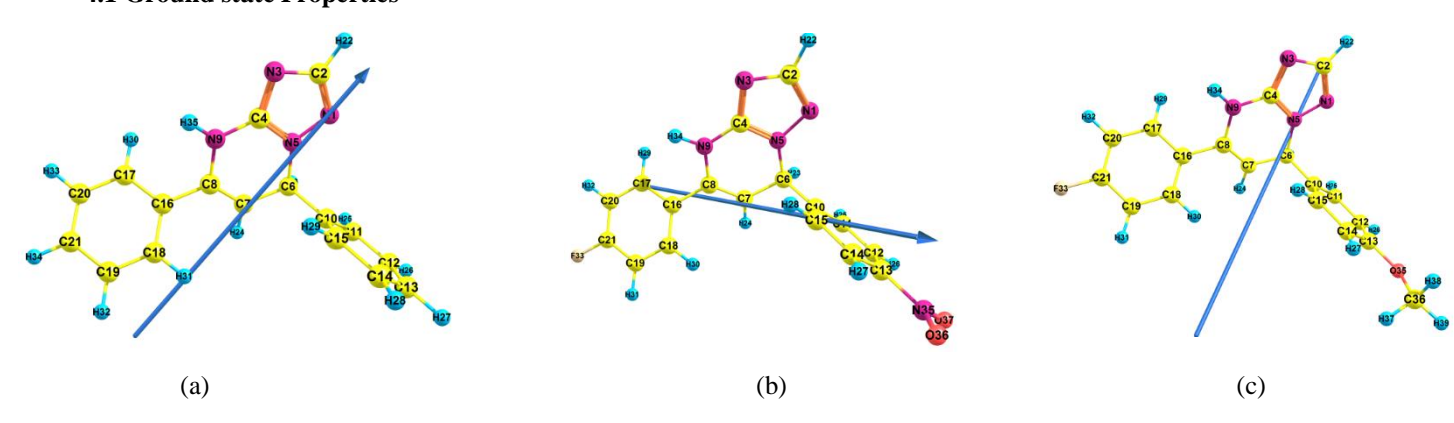
The electronic absorption spectra were measured using a Perkin Elmer Lambda 4B spectrophotometer using 1.0 cm fused quartz cells, where the spectrometer records linearly the percent of transmittance over the range 200-700 nm. Compounds 1,2,3,4,5,6, and 7 are dissolved in Dioxane at different concentrations of 0.000135 M, 0.0000625 M, 0.0000826 M, 0.0000924 M, 0.00008385, 0.0001588 M, 0.0000735M, respectively. Compounds 1,2,3,4,5,6, and 7 are dissolved in DMF at different concentrations of 0.0002 M, 0.00005 M, 0.00005 M, 0.0001 M, 0.0001455 M, 0.00014325 M, 0.0001485 M, respectively. The UV spectra of the dissolved compounds are recorded at ambient temperatures using a 1.0 cm fused quartz cell fitted into the spectrometer. The absorption spectra are acquired by displaying molar absorptivity versus wavelength.

### 3. Computational details

In this study, DFT (B3LYP) [39, 40] method was used. This function is a combination of the Becke's three parameters non-local exchange potential with the non-local correlation functional of lee et al. Full geometry optimization was performed using 6-311G (df, pd) as a basis set to generate the optimized structures and ground state properties of the studied triazolo [1,5-a] pyrimidine derivatives. The electronic transition properties, which include maximum excitation wavelength ( $\lambda_{max}$ ) and relative intensities (oscillator strengths, f), were obtained using the Time Dependent Density Functional Theory (TD-DFT) [41] at 6-311G(d,p) as a basis set. Theoretical absorption spectra were calculated in gas phase, Dioxane and DMF using TD-DFT, while in Dioxane and DMF, SCRF method was used, where the Polarizable Continuum Model (PCM) using the integral equation formalism variant (IEFPCM) is the default SCRF method [42, 43]. All calculations were performed using Gaussian 09W program package [44].

## 4. Result and Discussion

# 4.1 Ground state Properties



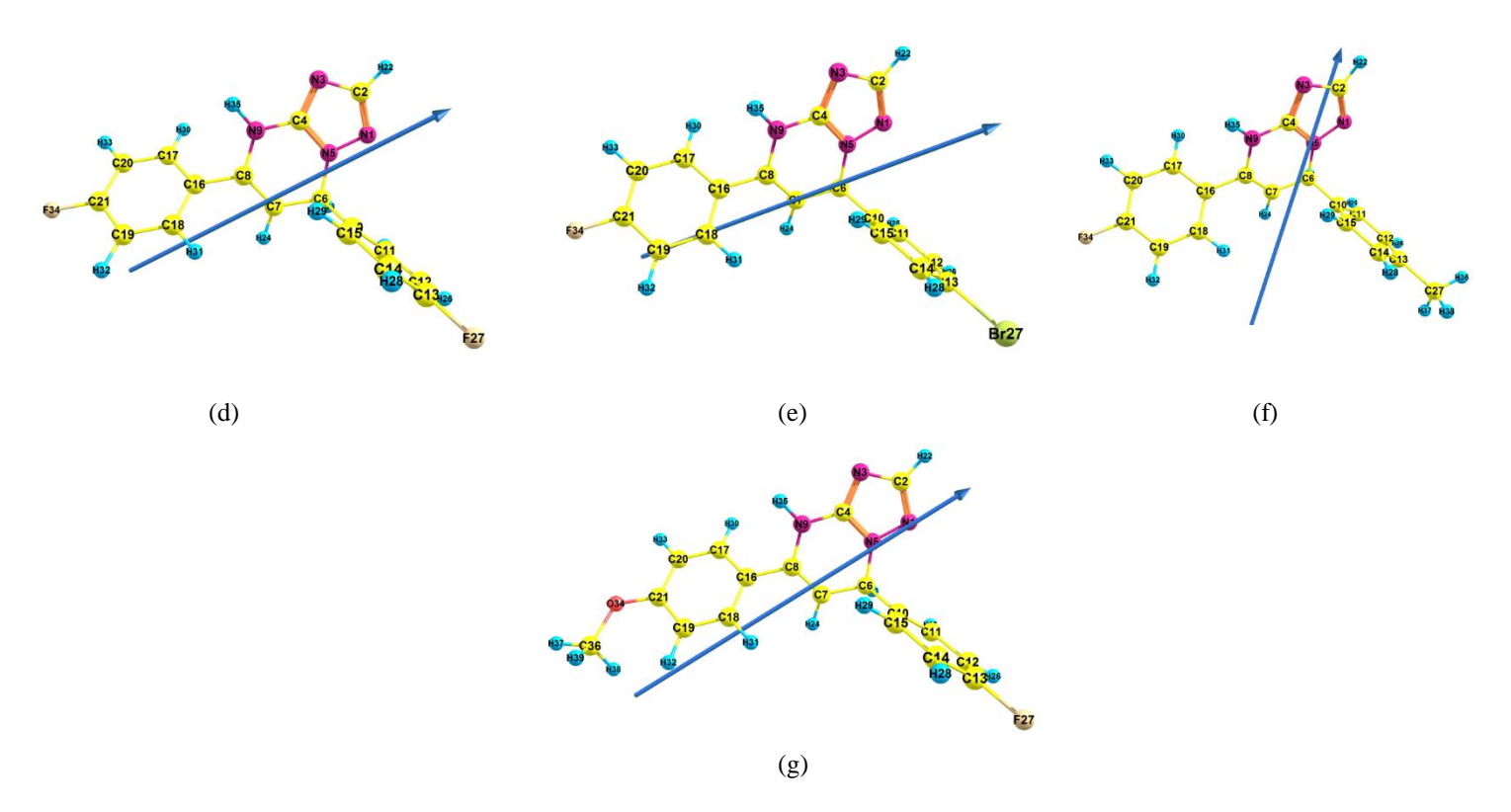


Figure 1. The optimized structure, perspective view of dipole moment of triazolo [1, 5-a] pyrimidine derivatives (a) 1, (b) 2, (c) 3, (d) 4, (e) 5, (f) 6, (g) 7 at B3LYP/6-311G (df, pd).

The full geometry optimization of the proposed molecules were carried out at the B3LYP/6-311G(df,pd) are presented in Fig. 1. The energies of HOMO, LUMO, energy gap  $E_g$  and dipole moment of all derivatives are presented in Fig. 2 and Table 1.

Table 1, Theoretical calculation of total energy,  $E_{HOMO}$ ,  $E_{LUMO}$ , Energy gap ( $E_g$ ) and dipole moment of compounds 1-7, calculated at B3LYP/6-311G(df,pd) in gas phase.

	culculated at D3L	711/0 3110(di,pd)	m gas phase.				_
G.S. Properties	1	2	3	4	5	6	7
E <sub>T</sub> (au)	-875.4766363	-1179.3053139	-1089.302333	-1074.0114824	-3548.2884968	-1014.0728369	-1089.3034277
$E_{HOMO} (eV)^a$	-5.803	-6.230	-5.806	-5.971	-6.021	-5.844	-5.764
$E_{LUMO} \left( \mathrm{eV} \right)^\mathrm{b}$	-1.277	-2.662	-1.234	-1.359	-1.423	-1.253	-1.081
$E_g$ (eV)	4.527	3.567	4.572	4.612	4.597	4.591	4.683
μ (debye)	4.00	5.36	3.43	2.85	3.05	2.88	5.63
$D(5-6-10-15)^{c}$	63.129	48.855	68.854	71.672	69.514	66.096	73.934
$D(9-8-16-17)^{c}$	36.513	37.991	36.295	36.843	36.268	36.720	36.235

<sup>&</sup>lt;sup>a</sup> I.E. = -  $E_{HOMO}$ <sup>b</sup> E.A. = -  $E_{LUMO}$ 

<sup>&</sup>lt;sup>c</sup>For numbering system (c.f. Fig. 1).

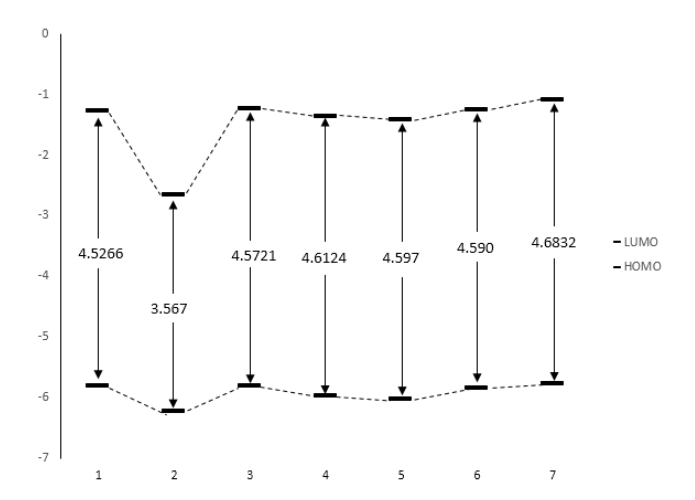
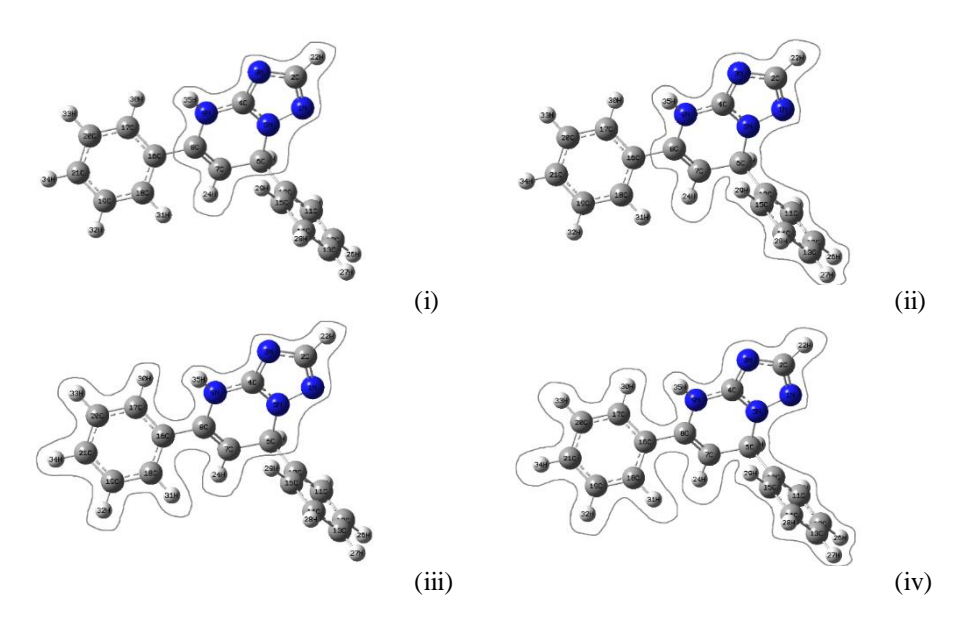


Figure 2. Energy of HOMO, LUMO and energy gap ( $E_g$ ), eV of the studied compounds at B3LYP/6-311G(df, pd) level of theory.

It is apparent from Fig. 1 that the optimized structures of compounds 1-7 are non-planar. To verify the non-planarity of these compounds it is found that the fused triazolo [1, 5-a] pyrimidine ring is almost planar, however the Ph-Y moiety is slightly out of the plane of the fused triazolo [1, 5-a] pyrimidine ring as indicated by the values of the dihedral angle D(9-8-16-17), which ranged from 36° to 38° for all the studied compounds, as shown in Table 1. Moreover, Ph-X is out of plane of the triazolo [1.5-a] pyrimidine fused ring by D(5-6-10-15), ranging from 49° to 74° for all the studied compounds (c.f. Table 1). One possible explanation of such non-planarity is the steric effect between Ph-X and the hydrogen atom binding to carbon atom (C6), as shown in Fig. 1. Moreover, there is another explanation why Ph-X is located out-of-plane, which involves the difference in the hybridization of C6, which has SP3 hybridization and flanked between SP2 carbons of Ph-X and pyrimidine ring. This difference in hybridization leads to geometrical changes at C6, giving rise to non-planarity of Ph-X. The insertion of F, Br, CH<sub>3</sub>, NO<sub>2</sub>, and OCH<sub>3</sub> groups in position 4 of either of the terminal phenyl groups doesn't make a noticeable change in the geometry of compounds 1-7, as shown in Fig. 1. The ionization energy, I.E., measures the donating property (oxidation power) of the molecule. The I.E. of compound 1 is calculated to be 5.803 eV, insertion of F atom in position 4 of Ph-Y and nitro group in position 4 of Ph-X results in the formation of compound 2 for which I.E. is 6.230 eV. The variation of I.E. with substituents is investigated by monitoring the calculated I.E. with variation of substituents in position 4 of Ph-X of compound 2. Insertion of OCH<sub>3</sub>, F, Br and CH<sub>3</sub> in position 4 of Ph-X of compound 2 results in the formation of compounds 3, 4, 5 and 6, respectively, which results in changing the I.E. to 5.806, 5.971, 6.021, and 5.844 eV, respectively. The reverse of the substituents of position 4 of Ph-X and Ph-Y of compound 3 results in the formation of compound 7, for which the I.E. is calculated to be 5.764 eV, indicating that the reverse of the position F and OCH<sub>3</sub> does not result in a significant change of I.E. The order of decreasing the I.E. (increasing the oxidation power) of the proposed molecules, is: 2>5>4>6>3>1>7, as shown in Table 1 and Fig. 2. The electron affinity, E.A, measures the accepting property (reduction power) of the molecule. The E.A. of compound 1 is calculated to be 1.277 eV. The analysis of E.A, indicates that the order of decrease of the reduction power is: 2 > 5 > 4 > 1 > 6 > 3 >7, as shown in Table 1 and Fig. 2. The band gap,  $E_g$  is the energy difference between  $E_{HOMO}$  and  $E_{LUMO}$ , it signifies the facile electron transition from  $E_{HOMO}$  to  $E_{LUMO}$ , i.e. the reactivity of molecule. The results in Table 1 and Fig. 2 show that the reactivity of these molecules increases in the order: 7 < 4 < 5 < 6 < 3 < 1 < 2. The dipole moment measures the polarizability of the molecule, where the order of decrease of the dipole moment is: 7 > 2 > 1 > 3 > 5 >6 > 4, as shown in Table 1 and Fig. 1.

#### 4.2 Electronic absorption spectra

The electronic absorption spectra of triazolo [1, 5-a] pyrimidine derivatives **1-7** studied in this workdepend on the type and extent of interaction between different moieties. Four possible types of interaction between subsystems can exist, as shown in scheme 2. For example: (i) no interaction between the fused triazolo [1, 5-a] pyrimidine ring and the two terminal phenyl groups Ph-X and Ph-Y; (ii) cross conjugation between Ph-X and triazolo [1, 5-a] pyrimidine; (iii) partial conjugation between Ph-Y and triazolo [1, 5-a] pyrimidine; (iv) full conjugation between the three subsystems Ph-X, Ph-Y and triazolo [1, 5-a] pyrimidine.



Scheme 2

## 4.2.1 Electronic absorption spectra of compound 1

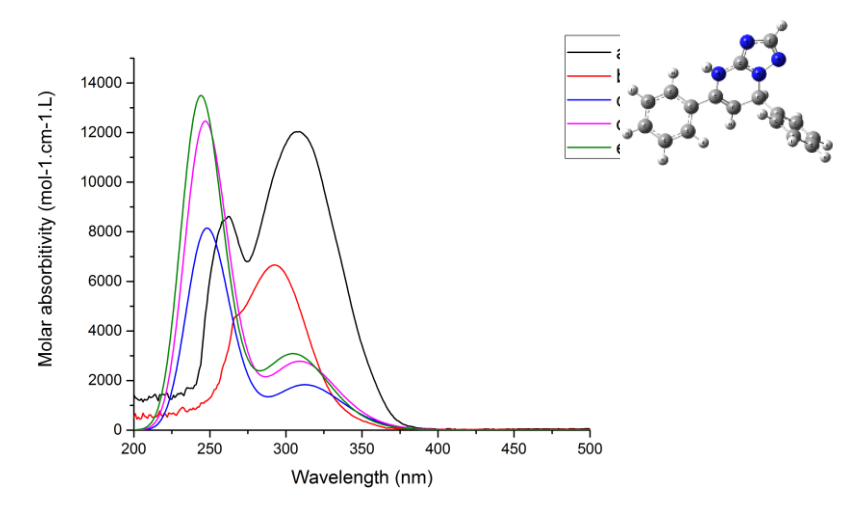


Figure 3. Electronic absorption spectra of compound 1; (a) experimental in Dioxane, (b) experimental in DMF, (c) theoretical in gas phase, (d) theoretical in Dioxane, (e) theoretical in DMF.

The experimental and theoretical electronic absorption spectra of compound 1 in Dioxane and DMF are presented in Fig. 3 and Table 2. The experimental UV spectrum in Dioxane shows two intense bands at 308 and 262 nm, increasing solvent polarity from Dioxane to DMF results in a noticeable blue shift of the first band and a small red shift of the second band, where the first band shifted to 293 nm and the second band shifted to 266 nm. Furthermore, increasing solvent polarity causes a marked decrease in the intensity of the two bands. The two observed bands are assigned as  $\pi$ - $\pi$ \* transitions, as reflected from the values of their molar absorptivity ( $\epsilon$  = 4000 - 13000).

Table 2, Experimental and theoretical UV spectra of compound 1, calculated at TD-B3LYP/6-311G(d,p).

Г	Theoretical												Experimen	tal	Assig.
Ex.	Gas phase				Dioxane				DMF			<u>.</u>	Dioxane	DMF	_
states	Config.	Coeff.	f	λ, nm	Config.	Coeff.	f	λ, nm	Config.	Coeff.	f	λ, nm	$\lambda_{max}$ , nm	$\lambda_{max}$ , nm	
S1	72 -> 73	0.700	0.0555	313.5	72 -> 73	0.701	0.0841	310.2	72 -> 73	0.699	0.0933	305.9	308.0	293.0	Electron delocal.
S2	72 -> 74	0.699	0.0019	282.1	72 -> 74	0.696	0.0031	276.1	72 -> 74 72 -> 75	0.675 -0.175	0.0009	270.6			
S3	72 -> 75	0.701	0.0011	269.1	72 -> 75	0.702	0.0023	268.6	72 -> 74 72 -> 75	0.162 0.675	0.0061	269.4			
S4	72 -> 76	0.697	0.0048	259.6	72 -> 76	0.696	0.0062	258.6	72 -> 76	0.696	0.0051	258.7			
S5	69 -> 73 71 -> 73	0.113 0.671	0.2468	248.0	71 -> 73	0.678	0.3758	246.8	70 -> 73 71 -> 73	-0.112 0.669	0.4037	244.1	262.0	266.0	Electron delocal.
S6	65 -> 74 68 -> 73 69 -> 74 70 -> 74 71 -> 74	-0.124 0.486 0.145 0.197 -0.412	0.0007	240.3	65 -> 74 68 -> 73 70 -> 74 71 -> 74 72 -> 74	0.113 0.514 0.202 -0.387 -0.112	0.0035	239.5	68 -> 73 70 -> 74 71 -> 74 71 -> 75 72 -> 74	0.534 -0.140 -0.325 -0.183 0.121	0.0088	238.8			

To help predicting and assigning the origin of the experimental spectrum of compound 1, the theoretical gas phase transitions of the various subsystems a, b and c are calculated using TD-B3LYP/6-311G(d,p), which are presented in Fig. 4 and Table 3.

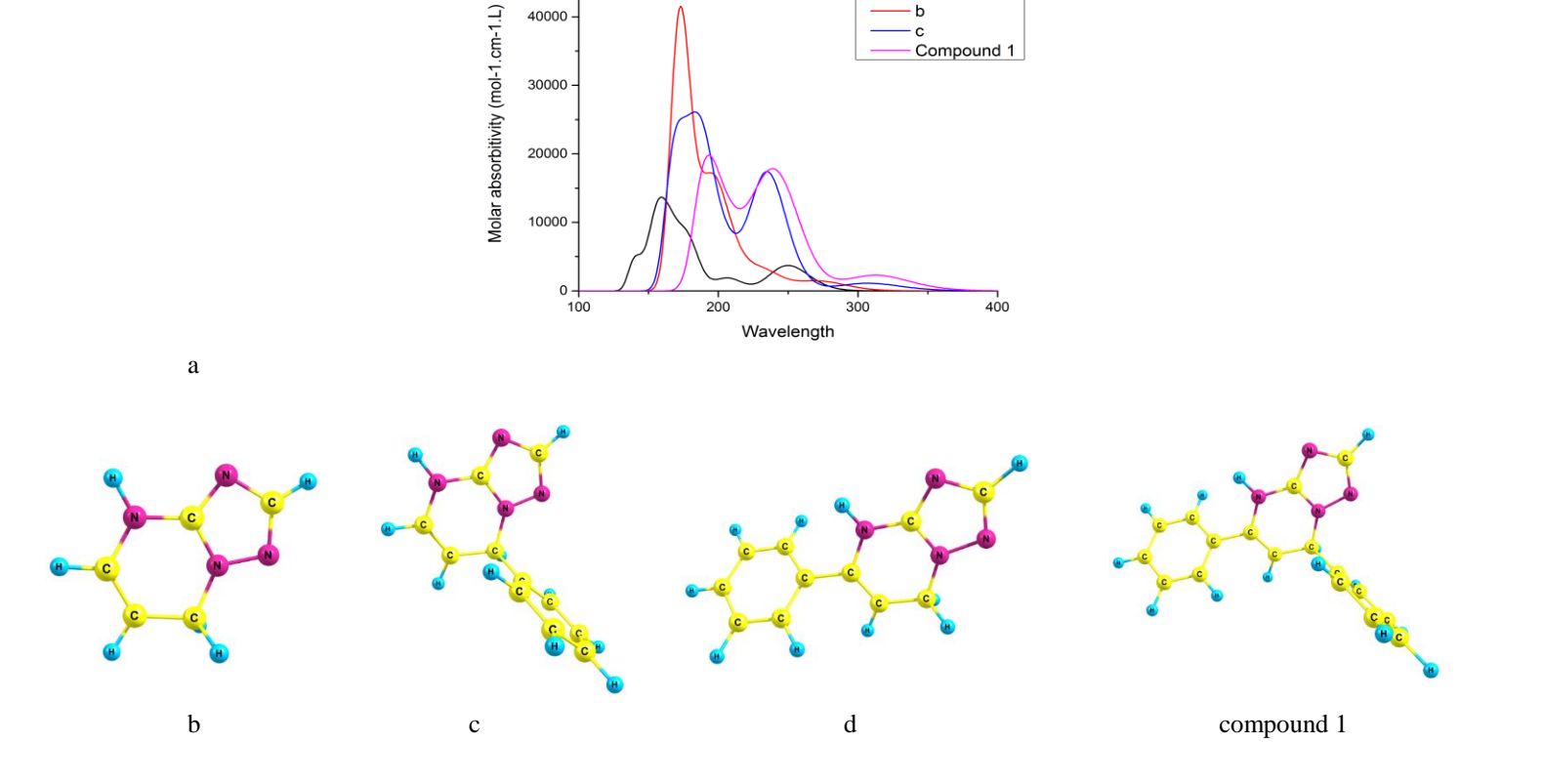


Figure 4. Theoretical UV-spectra calculated at TD-DFT B3LYP/6-311G(d,p) level of theory of : (a) 4,7-dihydro-[1,2,4]triazolo[1,5-a]pyrimidine; (b) 7-phenyl-4,7-dihydro-[1,2,4]triazolo[1,5-a]pyrimidine; (c) 5-phenyl-4,7dihydro-[1,2,4]triazolo[1,5-a]pyrimidine; (compound 1) 5,7-diphenyl-4,7-dihydro-[1,2,4]triazolo[1,5-a]pyrimidine.

Table 3, Theoretical vertical excitations of Compound 1 and its subsystems calculated at TD- B3LYP/6-311G(d,p)

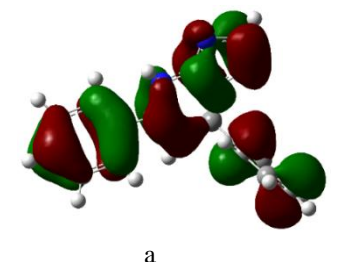
in	gas	phase*

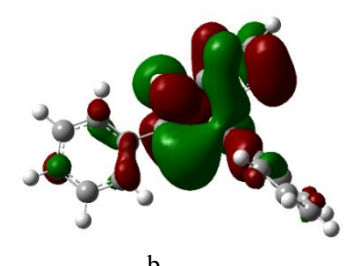
Single point vertical excitation	a	b	c	Compound 1
1	250.0	263.4	281.7	259.6
2		274.9	308.1	269.1
3				282.1
4				313.5

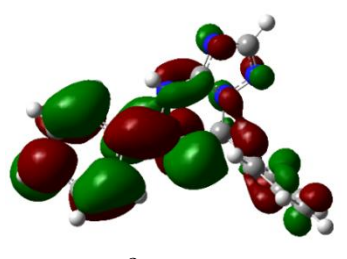
<sup>\*</sup> Structures of Compound 1 and its subsystems a, b and c are shown in Fig. 4.

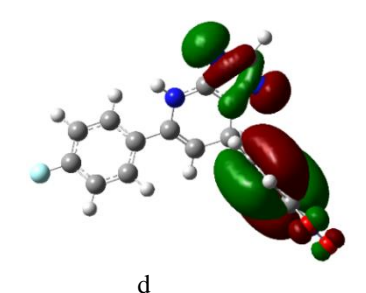
For subsystem a, one transition is computed at 250 nm; subsystem b, two transitions are computed at 263.4, and 274.9 nm; subsystem c, two transitions are computed at 281.7, and 308.1 nm; compound 1, four transitions are computed at 259.6, 269.1, 282.1, and 313.5 nm. The correlation of the theoretical transitions of the various subsystems, shown in Table 3, indicates that the transition at 281.7 nm of subsystem c correlates with the transition at 282.1 nm of compound 1. Moreover, the transition at 308.1 nm of subsystem c correlates with that at 313.5 nm of compound 1. This indicates that the partial conjugation of Ph-Y and triazolo [1, 5-a] pyrimidine of subsystem c reproduces the full conjugation of compound 1, which verifies the negligible influence of the interaction of Ph-X on the triazolo [1, 5-a] pyrimidine due to the non-planarity of the former with the latter (c.f. scheme 2).

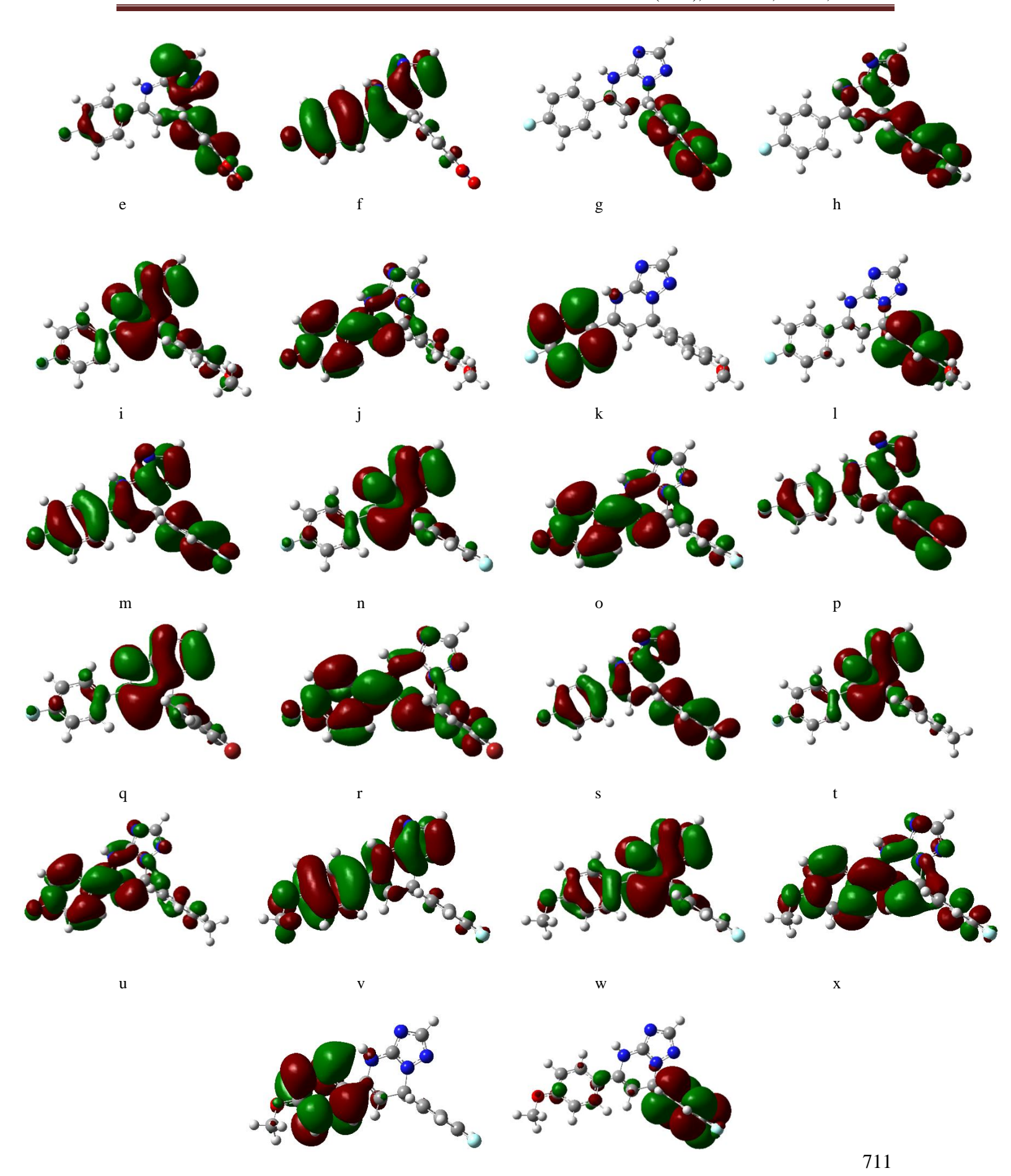
In order to account for the experimentally observed UV Spectra of compound 1 in Dioxane and DMF, one needs to consider the theoretically calculated vertical transitions using TD/B3LYP/6-311G(d,p) level. In Dioxane, the band appearing in the experimental spectrum at 308 nm is reproduced theoretically using Dioxane as a solvent by the vertical excitation S1 at 310.2 nm, as shown in Table 2, which involves orbitals  $\Phi_{72}$  and  $\Phi_{73}$ . The observed wavelength in the UV spectrum is 2.2 nm lower than the calculated wavelength. Increasing solvent polarity in DMF, causes  $\lambda_{max}$  of this band to appear at 293 nm. The theoretical calculation in DMF reproduces the wavelength of this band at 305.9 nm (S1), showing that the orbitals  $\Phi_{72}$  and  $\Phi_{73}$  are also involved in this transition, indicating that the calculated wavelength is higher than the observed wavelength. Theoretical gas phase calculations reproduce this band at 313.5 nm (S1), which also involves  $\Phi_{72}$  and  $\Phi_{73}$ , indicating that gas phase calculations give higher wavelength than the theoretical wavelength calculated using Dioxane or DMF as a solvent. The second band, experimentally observed at 262 nm in Dioxane, is reproduced theoretically in Dioxane at 246.8 nm (S5), which is lower than the experimental wavelength, which involves the orbitals  $\Phi_{71}$  and  $\Phi_{73}$  in the transition. In DMF, this band appears at 266 nm, where theoretical calculations in DMF reproduce this band at 244.1 nm (S5), which is lower than the observed wavelength, which involves the orbitals  $\Phi_{71}$  and  $\Phi_{73}$  in the transition. Comparing with gas phase, theoretical calculations give a transition at 248.0 nm (S5), which is higher than the theoretical wavelengths calculated in Dioxane or DMF, it also involves orbitals  $\Phi_{71}$  and  $\Phi_{73}$ . The nature of the electronic transition can be inferred from examining the electron density contours of molecular orbitals, which are shown in Fig. 5 for all the studied compounds. The three orbitals  $\Phi_{71}$ ,  $\Phi_{72}$  and  $\Phi_{73}$ , involved in the theoretical transitions of compound 1, are shown in Fig. 5a, 5b and 5c, respectively, where the first band, involving  $\Phi_{72}^{-1}$   $\Phi_{73}$ , and the second band, involving  $\Phi_{71}^{-1}$   $\Phi_{73}$ , show a delocalization of electron density.











y

Figure 5. Electron density contour of (a)  $\Phi_{71}$ , (b)  $\Phi_{72}$ , (c)  $\Phi_{73}$  of **1**; (d)  $\Phi_{84}$ , (e)  $\Phi_{85}$ , (f)  $\Phi_{86}$ , (g)  $\Phi_{88}$  of **2**; (h)  $\Phi_{83}$ , (i)  $\Phi_{84}$ , (j)  $\Phi_{85}$ , (k)  $\Phi_{86}$ , (l)  $\Phi_{87}$  of **3**; (m)  $\Phi_{79}$ , (n)  $\Phi_{80}$ , (o)  $\Phi_{81}$  of **4**; (p)  $\Phi_{92}$ , (q)  $\Phi_{93}$ , (r)  $\Phi_{94}$  of **5**; (s)  $\Phi_{79}$ , (t)  $\Phi_{80}$ , (u)  $\Phi_{81}$  of **6**; (v)  $\Phi_{83}$ , (w)  $\Phi_{84}$ , (x)  $\Phi_{85}$ , (y)  $\Phi_{86}$ , (z)  $\Phi_{87}$  of **7**.

## 4.2.2 Electronic absorption spectra of compound 2

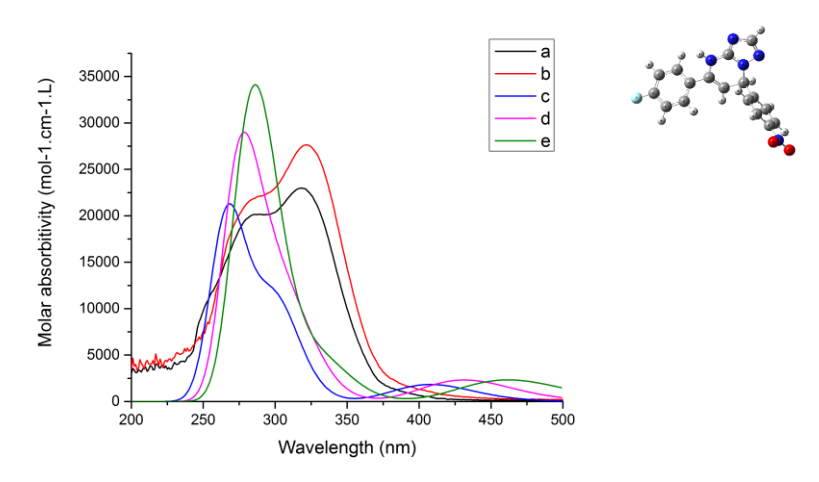


Figure 6. Electronic absorption spectra of compound 2; (a) experimental in Dioxane, (b) experimental in DMF, (c) theoretical in gas phase, (d) theoretical in Dioxane, (e) theoretical in DMF.

Compound 2 results by inserting of  $NO_2$  group in position X and F atom in position Y in Ph-X and Ph-Y of compound 1. As in compound 1, the experimental and theoretical electronic absorption spectra of compound 2 in Dioxane and DMF are shown in Fig. 6 and Table 4.

Table 4, Experimental and theoretical UV spectra of compound 2, calculated at TD-B3LYP/6-311G(d,p).

E	Theoretical Experimental														- Assig.
Ex.	Gas phase				Dioxane				DMF			<u> </u>	Dioxane	DMF	- Assig.
states	Config.	Coeff.	f	λ, nm	Config.	Coeff.	f	λ, nm	Config.	Coeff.	f	λ, nm	$\lambda_{max}$ , nm	$\lambda_{max}$ , nm	
S1	87 -> 88	0.704	0.0210	407.9	87 -> 88	0.705	0.0266	431.4	87 -> 88	0.705	0.0267	461.9			
S2	80 -> 88	0.129	0.0000	323.4	79 -> 88	0.307	0.0000	322.2	86 -> 88	0.704	0.0463	333.9			
	81 -> 88	0.679			80 -> 88	0.620									
	81 -> 92	-0.119			80 -> 92	-0.100									
S3	86 -> 88	0.700	0.0490	304.1	86 -> 88	0.704	0.0592	317.7	79 -> 88	0.694	0.0001	320.8	319.0	322.0	CT-band
									79 -> 92	-0.102					
S4	87 -> 89	0.690	0.0691	299.4	87 -> 89	0.691	0.0935	299.4	83 -> 88	0.137	0.1033	298.8			
									84 -> 88	-0.167					
									87 -> 89	0.655					
									87 -> 90	-0.120					
S5	87 -> 90	0.699	0.0048	287.3	83 -> 88	0.587	0.0194	285.9	83 -> 88	0.586	0.0338	295.3			
					85 -> 88	-0.290			84 -> 88	-0.297					
					85 -> 91	-0.104			87 -> 89	-0.209					
					87 -> 91	-0.174									
S6	78 -> 88	0.689	0.0002	286.3	78 -> 88	0.687	0.0014	283.5	78 -> 88	-0.104	0.2273	283.3			
	78 -> 92	-0.114			78 -> 92	-0.105			83 -> 88	0.251					
									84 -> 88	0.538					
									87 -> 90	-0.351					
S7	83 -> 88	0.159	0.0064	279.0	87 -> 90	0.691	0.0103	282.7	85 -> 88	0.582	0.0036	280.4			
	84 -> 88	0.409							87 -> 90	0.173					
	85 -> 88	-0.139							87 -> 91	0.349					
	87 -> 91	0.515													

S8	83 -> 88 84 -> 88 85 -> 88	-0.123 -0.388 0.309	0.0114	275.2	85 -> 88 87 -> 91	-0.306 0.625	0.0357	278.9	78 -> 88 87 -> 90	0.630 -0.262	0.0007	279.9			
S9	87 -> 91 84 -> 88 85 -> 88 87 -> 91	0.462 0.318 0.604 -0.108	0.1939	268.0	83 -> 88 85 -> 88 87 -> 91	0.338 0.549 0.241	0.2452	275.0	78 -> 88 83 -> 88 84 -> 88 85 -> 88	0.271 0.225 0.279 -0.158	0.0718	279.5	286.0	287.0	Electron delocal.
									87 -> 89 87 -> 90	0.102 0.498					

In Dioxane, the experimental spectrum is composed of two bands at 319 and 286 nm. Increasing solvent polarity from Dioxane to DMF results in a small red shift of the two bands, where the first band shifted to 322 nm and the second band shifted to 287 nm. Furthermore, increasing solvent polarity causes an increase in the intensity of both bands. The two observed bands are assigned as  $\pi$ - $\pi$ \* transitions. To interpret the experimentally observed UV Spectra of compound 2 in Dioxane and DMF, the theoretically calculated vertical transitions using TD/B3LYP/6-311G(d,p) level is considered. In Dioxane, the band appearing in the experimental spectrum at 319 nm is reproduced theoretically using Dioxane as a solvent at 317.7 nm (S3), showing a fair agreement with the observed  $\lambda_{max}$ , which involves orbitals  $\Phi_{86}$  and  $\Phi_{88}$ . Increasing solvent polarity in DMF, makes this band to appear at 322 nm. Theoretical calculations of vertical excitation in DMF reproduce this band at 333.9 nm (S2), showing that the same orbitals are involved in this transition as in Dioxane calculations, indicating that the calculated wavelength is higher than the observed wavelength. Gas phase calculations reproduce this band at 304.1 nm (S3), which also involves the same orbitals as in DMF and Dioxane, indicating that the gas phase calculations give a lower wavelength than that calculated using DMF or Dioxane as a solvent. The second band  $\lambda_{max}$ , observed at 286 nm in Dioxane, is reproduced theoretically in Dioxane at 275.0 nm (S9), indicating that the orbitals  $\Phi_{85}$  and  $\Phi_{88}$  are involved in this transition. In DMF, this band appears at 287 nm, where theoretical calculations in DMF reproduce this band at 283.3 nm (S6), which shows a fair agreement with the experimental wavelength, where the orbitals  $\Phi_{84}$  and  $\Phi_{88}$  are involved in this transition. Theoretical gas phase calculations give a value of 268.0 nm (S9) for this band, which involves orbitals  $\Phi_{85}$  and  $\Phi_{88}$  in the transition as in Dioxane. Moreover, theoretical gas phase wavelength for this transition is found to be lower than the theoretical wavelengths calculated in Dioxane or DMF. The four orbitals  $\Phi_{84}$ ,  $\Phi_{85}$ ,  $\Phi_{86}$ , and  $\Phi_{88}$  are involved in the theoretical transitions of compound 2, as shown in Fig. 5d, 5e, 5f and 5g, respectively, where the first band, involving  $\Phi_{86}$  and  $\Phi_{88}$  orbitals for gas phase , Dioxane and DMF, shows a charge transfer CT character, while the second band, involving  $\Phi_{84}$ ,  $\Phi_{85}$  and  $\Phi_{88}$  orbitals, shows a delocalization of electron density character when both configurations,  $\Phi_{84}^{-1}$   $\Phi_{88}$  in DMF, and  $\Phi_{85}^{-1}$   $\Phi_{88}$  in gas phase and Dioxane, are involved.

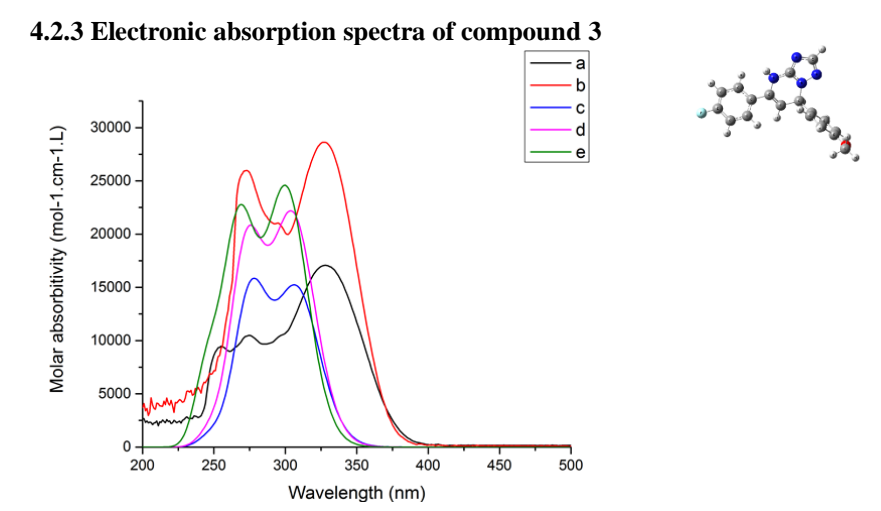


Figure 7. Electronic absorption spectra of compound 3; (a) experimental in Dioxane, (b) experimental in DMF, (c) theoretical in gas phase, (d) theoretical in Dioxane, (e) theoretical in DMF.

Compound 3 results by keeping F atom in Ph-Y and inserting OCH<sub>3</sub> group in position X of compound 2. The experimental and theoretical electronic absorption spectra of compound 3 in Dioxane and DMF are shown in Fig. 7 and Table 5.

Table 5, Experimental and theoretical UV spectra of compound 3, calculated at TD-B3LYP/6-311G(d,p).

E	Theoretica	1			Experimental										
Ex. states	Gas phase				Dioxane				DMF				Dioxane	DMF	Assig.
states	Config.	Coeff.	f	λ, nm	Config.	Coeff.	f	λ, nm	Config.	Coeff.	f	λ, nm	$\lambda_{max}$ , nm	$\lambda_{max}$ , nm	="
S1	84 -> 85	0.696	0.0692	309.4	84 -> 85	0.698	0.1036	306.5	84 -> 85	0.697	0.1179	301.7	328.0	327.0	Electron delocal.
S2	84 -> 86	0.696	0.0064	300.1	84 -> 86	0.696	0.0095	293.3	84 -> 86	0.695	0.0116	285.4	297.0	295.0	CT-band
S3	83 -> 85	0.698	0.0755	276.6	83 -> 85	0.697	0.0965	273.8	83 -> 85 84 -> 87	-0.341 0.609	0.0242	268.9	275.0	273.0	CT-band
S4	84 -> 87	0.700	0.0021	266.3	84 -> 87	0.700	0.0034	266.5	83 -> 85 84 -> 87	0.605 0.347	0.0813	268.3			
S5	83 -> 86	0.699	0.0012	258.5	83 -> 86	0.695	0.0020	253.0	83 -> 87 84 -> 88	0.253 0.638	0.0094	250.9			
S6	83 -> 87 84 -> 88	0.255 0.637	0.0065	249.9	83 -> 87 84 -> 88	0.282 0.625	0.0091	250.1	81 -> 85 81 -> 88 83 -> 86 83 -> 87 83 -> 88 84 -> 88	-0.115 0.160 -0.394 0.459 0.116 -0.215	0.0352	245.7			
S7	81 -> 85 81 -> 88 83 -> 87 83 -> 88 84 -> 88	-0.180 0.211 0.556 0.152 -0.263	0.0225	244.9	81 -> 85 81 -> 88 83 -> 87 83 -> 88 84 -> 88	-0.152 0.195 0.556 0.145 -0.290	0.0352	245.3	80 -> 85 81 -> 88 82 -> 86 83 -> 86 83 -> 87 84 -> 88	-0.113 0.110 -0.137 0.545 0.341 -0.136	0.0091	244.9	255.0		Electron delocal.

The observed spectrum of compound 3 in Dioxane is composed of four bands appearing at 328, 297, 275 and 255 nm. Compound 3 in DMF exhibits three bands at 327, 295 and 273 nm, where the fourth band, observed in Dioxane, disappeared in the experimental UV spectrum in DMF. The change of solvent polarity from Dioxane to DMF does not result in a significant change in wavelength for all the observed bands. The intensity of all bands is increased upon increasing solvent polarity. All bands are assigned to have  $\pi$ - $\pi$ \* character. TD/B3LYP/6-311G(d,p) vertical excitation calculations helped in the interpretation of the observed UV Spectra of compound 3 in Dioxane, which gives excitations at 306.5 (S1), 293.3 (S2), 273.8 (S3) and 245.3 (S7) nm, showing a satisfactory agreement with the second and third bands, and a fair agreement with the fourth band. Vertical excitation calculations of compound 3 in DMF gives four bands at 301.7 (S1), 285.4 (S2), 268.3 (S4) and 245.7 (S6) nm, which shows a fair agreement with the second and third bands, while the fourth band is reproduced theoretically and unobserved experimentally in DMF. In gas phase, vertical excitation calculations of compound 3 reproduce the four bands at 309.4 (S1), 300.1 (S2), 276.6 (S3) and 244.9 (S7) nm. The vertical excitation calculations indicate that the orbitals  $\Phi_{84}$  and  $\Phi_{85}$  are involved in the transition for the first band in gas phase, Dioxane, and DMF, as shown in Fig. 5i and 5j, which show a delocalization of electron dentistry. The orbitals  $\Phi_{84}$  and  $\Phi_{86}$  are involved in the transition for the second band in gas phase, Dioxane and DMF, as shown in Fig. 5i and 5k, which show a charge transfer CT character. The calculations in gas phase, Dioxane and DMF elucidate that the orbitals  $\Phi_{83}$  and  $\Phi_{85}$  are involved in the transition for the third band, showing a charge transfer character, as shown in Fig. 5h and 5j. Forthe fourth band, the orbitals involved in the theoretical vertical excitation for gas phase, Dioxane and DMF, are  $\Phi_{83}$  and  $\Phi_{87}$ , as shown in Fig. 5h and 51, where electron density delocalization character manifests itself.

### 4.2.4 Electronic absorption spectra of compound 4

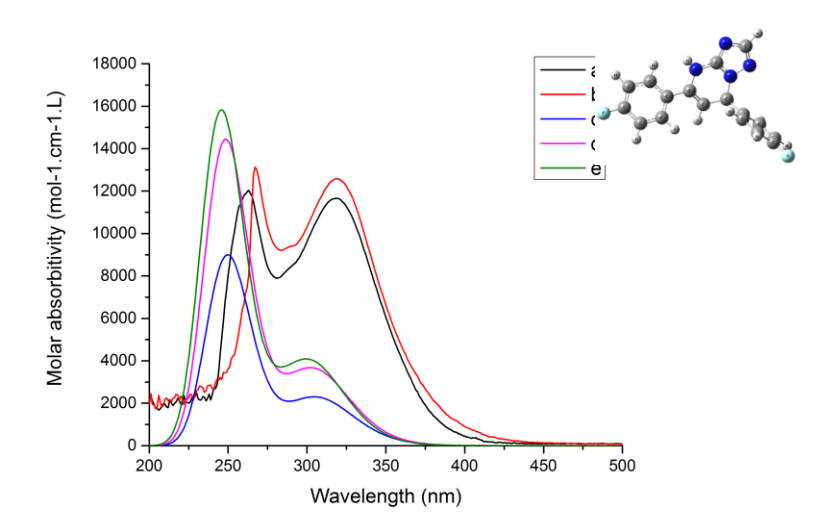


Figure 8. Electronic absorption spectra of compound 4; (a) experimental in Dioxane, (b) experimental in DMF, (c) theoretical in gas phase, (d) theoretical in Dioxane, (e) theoretical in DMF.

Inserting F atom in position X of compound 2 results in the formation of compound 4. The experimental and theoretical electronic absorption spectra of compound 4 in Dioxane and DMF are shown in Fig. 8 and Table 6.

Table 6, Experimental and theoretical UV spectra of compound 4, calculated at TD-B3LYP/6-311G(d,p).

	Theoretical	ĺ						•				•	Experimen	tal	Assig.
Ex.	Gas phase				Dioxane				DMF				Dioxane	DMF	
states	Config.	Coeff.	f	λ, nm	Config.	Coeff.	f	$\lambda$ , nm	Config.	Coeff.	f	$\lambda,nm$	$\lambda_{\text{max}}$ , nm	$\begin{array}{c} \lambda_{max}  , \\ nm \end{array}$	
S1	80 -> 81	0.698	0.0518	307.3	80 -> 81	0.699	0.0834	305.3	80 -> 81	0.698	0.0932	302.3	319.0	319.0	Electron delocal.
S2	80 -> 82	0.700	0.0044	295.3	80 -> 82	0.700	0.0069	288.9	80 -> 82	0.698	0.0088	282.6			ļ
S3	80 -> 83	0.702	0.0001	273.5	80 -> 83	0.702	0.0003	274.4	80 -> 83	0.701	0.0003	276.4			1
S4	80 -> 84	0.697	0.0020	259.4	80 -> 84	0.695	0.0032	258.3	80 -> 84	0.692	0.0034	258.9			1
S5	78 -> 81 79 -> 81	0.129 0.672	0.2129	249.8	79 -> 81	0.675	0.3458	248.5	78 -> 81 79 -> 81	-0.131 0.663	0.3833	245.7	263.0	267.0	Electron delocal.
S6	75 -> 81 78 -> 82	0.332	0.0079	244.2	76 -> 81 78 -> 82	0.358 0.287	0.0085	242.0	76 -> 81 78 -> 82	0.391 0.222	0.0048	239.7			
	79 -> 82	0.517			79 -> 82	0.513			79 -> 82	0.514					'

In Dioxane, the experimental spectrum is composed of two bands at 319 and 263 nm. In DMF, the two bands are observed at 319 and 267 nm. The change of solvent polarity to DMF results in no change of band maximum ( $\lambda_{max}$ ) for the first band, which implies solvent independence, while the second band is red shifted by 4 nm. The increase of solvent polarity results in a slight increase in the intensity of the two bands. The two observed bands are assigned to have  $\pi$ - $\pi$ \* character. To explain the observed UV Spectra of compound 4 in Dioxane and DMF, vertical excitations are calculated, which give 305.3 nm (S1) for the first band, using Dioxane as a solvent, where the theoretical transition involves orbitals  $\Phi_{80}$  and  $\Phi_{81}$ . Theoretical calculations in DMF give 302.3 nm (S1) for the same band, where the orbitals involved in this transition are the same as in Dioxane. Gas phase vertical excitations reproduce this band at 307.3 nm (S1), which also involves the orbitals  $\Phi_{80}$  and  $\Phi_{81}$ . The second band observed at 263 nm in Dioxane, is reproduced theoretically at 248.5 nm (S5), where calculations in Dioxane indicate that orbitals  $\Phi_{79}$  and  $\Phi_{81}$  are involved in this transition. Theoretical calculations in DMF show that, this band appears at 245.7 nm (S5), which is lower than the experimental wavelength, where calculations show that the orbitals involved in this transition are the same as in Dioxane. Gas phase calculations give a transition at 249.8 nm (S5), indicating that the orbitals involved in the transition are also  $\Phi_{79}$  and  $\Phi_{81}$  as in both solvents. The orbitals involved in the theoretical

transitions of compound **4** are  $\Phi_{79}$ ,  $\Phi_{80}$  and  $\Phi_{81}$ , as shown in Fig. 5m, 5n and 5o. Both first and second bands, involving  $\Phi_{80}^{-1}$   $\Phi_{81}$  and  $\Phi_{79}^{-1}$   $\Phi_{81}$  transition configurations, respectively, for gas phase, Dioxane and DMF, show electron delocalization character.

### 4.2.5 Electronic absorption spectra of compound 5

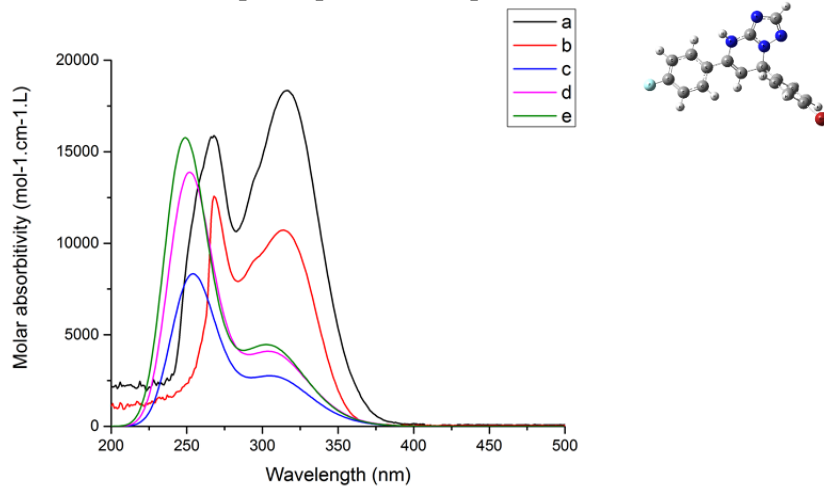


Figure 9. Electronic absorption spectra of compound 5; (a) experimental in Dioxane, (b) experimental in DMF, (c) theoretical in gas phase, (d) theoretical in Dioxane, (e) theoretical in DMF.

Replacing F atom in position X of compound 4 with Br atomresults in the formation of compound 5. The experimental and theoretical electronic absorption spectra of compound 5 in Dioxane and DMF are shown in Fig. 9 and Table 7.

Table 7, Experimental and theoretical UV spectra of compound 5, calculated at TD-B3LYP/6-311G(d,p).

Ex.	Theoretica	l .											Experimen	tai	Assig.
states	Gas phase				Dioxane				DMF				Dioxane	DMF	Assig.
states	Config.	Coeff.	f	λ, nm	Config.	Coeff.	f	λ, nm	Config.	Coeff.	f	λ, nm	$\lambda_{max}$ , nm	$\lambda_{max}$ , nm	
S1	93 -> 94	0.697	0.0618	309.2	93 -> 94	0.697	0.0926	308.1	93 -> 94	0.695	0.1009	306.6	317.0	314.0	Electron delocal.
S2	93 -> 95	0.700	0.0043	293.7	93 -> 95	0.700	0.0062	287.8	93 -> 95	0.702	0.0019	284.1			
S3	93 -> 96	0.703	0.0013	279.5	93 -> 96	0.702	0.0034	280.9	93 -> 96	0.697	0.0116	281.2			
S4	93 -> 97	0.698	0.0010	268.1	93 -> 97	0.697	0.0022	267.5	93 -> 97	0.694	0.0048	267.5			
S5	90 -> 96 92 -> 94	0.104 0.673	0.1976	254.2	90 -> 96 92 -> 94	0.105 0.670	0.3328	251.9	90 -> 95 92 -> 94	0.104 0.655	0.3786	248.8	268.0	268.0	Electron delocal.
S6	88 -> 94 91 -> 95 92 -> 95	0.330 -0.423 0.432	0.0080	244.3	89 -> 94 89 -> 97 91 -> 95 92 -> 95	-0.357 0.109 -0.385 0.437	0.0088	242.1	91 -> 98 93 -> 98	0.112 0.689	0.0070	244.0			

Similar to compound **4**, the experimental spectrum of compound **5** is composed of two bands, where their values are close to their corresponding bands in compound **4**. In Dioxane, the two bands observed at 317 and 268 nm, where in DMF the two bands appear at 314 and 268 nm. The change of solvent polarity from Dioxane to DMF results in an insignificant blue shift for the first band, while the second band shows no band shifting. Unlike compound **4**, the increase of solvent polarity results in a decrease in the intensity of the bands. The two observed bands are assigned to have  $\pi$ - $\pi$ \* character. All the observed transitions, theoretically calculated vertical excitations and their assignments are shown in Table 7. The orbitals,  $\Phi_{92}$ ,  $\Phi_{93}$  and  $\Phi_{94}$ , involved in the theoretical transitions of compound **5**, are displayed in Fig. 5p, 5q and 5r.

## 4.2.6 Electronic absorption spectra of compound 6

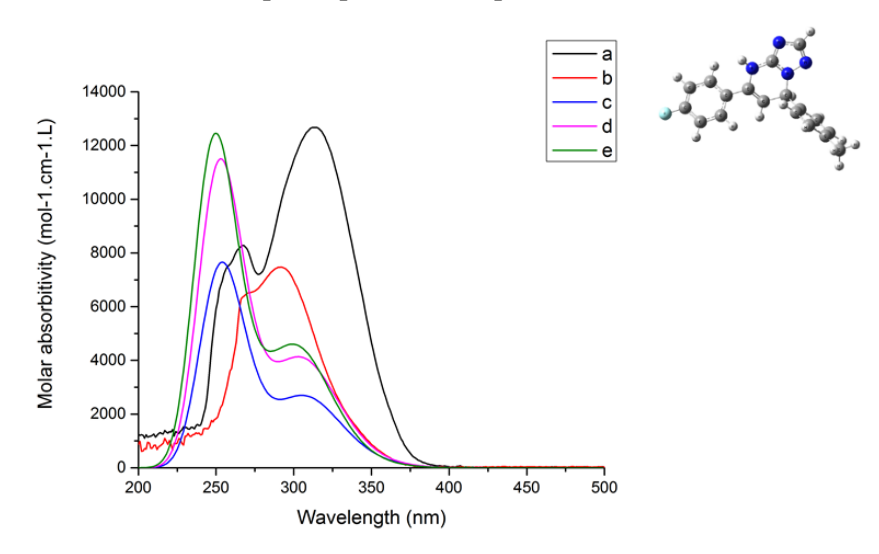


Figure 10. Electronic absorption spectra of compound **6**; (a) experimental in Dioxane, (b) experimental in DMF, (c) theoretical in gas phase, (d) theoretical in Dioxane, (e) theoretical in DMF.

Inserting CH<sub>3</sub> group in position X of compound **2** results in the formation of compound **6**. The experimental and theoretical electronic absorption spectra of compound **6** in Dioxane and DMF are shown in Fig. 10 and Table 8.

Table 8, Experimental and theoretical UV spectra of compound 6, calculated at TD-B3LYP/6-311G(d,p).

Ex.	Theoretical	Theoretical													- Assig.
	Gas phase				Dioxane				DMF				Dioxane	DMF	Assig.
	Config.	Coeff.	f	λ, nm	Config.	Coeff.	f	λ, nm	Config.	Coeff.	f	λ, nm	$\lambda_{max}$ , nm	$\lambda_{max}$ , nm	
S1	80 -> 81	0.698	0.0599	308.8	80 -> 81	0.699	0.0924	306.9	80 -> 81	0.698	0.1035	303.1	313.0	291.0	Electron delocal.
S2	80 -> 82	0.700	0.0048	298.4	80 -> 82	0.700	0.0075	291.7	80 -> 82	0.698	0.0095	284.4			
S3	80 -> 83	0.703	0.0009	267.7	80 -> 83 80 -> 84	0.694 0.114	0.0017	261.9	80 -> 83 80 -> 84	0.695 0.108	0.0020	263.1			
S4	79 -> 81 80 -> 84	0.280 0.632	0.0261	255.2	80 -> 83 80 -> 84	-0.113 0.684	0.0056	257.9	80 -> 83 80 -> 84	-0.108 0.684	0.0039	258.1			
S5	79 -> 81 80 -> 84	0.627 -0.290	0.1552	254.0	79 -> 81	0.685	0.2692	253.0	79 -> 81	0.679	0.2969	249.6	267.0	268.0	Electron delocal.
S6	74 -> 81 75 -> 81 78 -> 82 79 -> 82	0.126 0.281 -0.351 0.510	0.0079	245.3	76 -> 81 78 -> 82 79 -> 82	0.341 -0.379 0.458	0.0089	242.7	76 -> 81 78 -> 82 79 -> 82	-0.383 -0.373 0.427	0.0055	240.0			

In Dioxane, the experimental spectrum is composed of two bands at 313 and 267 nm. Increasing solvent polarity from Dioxane to DMF results in a noticeable blue shift by 22 nm for the first band, where the first band shifted to 291 nm and the second band shifted to 268 nm, it also results in decreasing of the intensity of both bands. The two observed bands are assigned as  $\pi$ - $\pi$ \* transitions. All the observed transitions, theoretically calculated vertical excitations and their assignments are shown in Table 8. The three orbitals,  $\Phi_{79}$ ,  $\Phi_{80}$  and  $\Phi_{81}$ , involved in the theoretical transitions of compound 6, are shown in Fig. 5s, 5t and 5u.

## 4.2.7 Electronic absorption spectra of compound 7



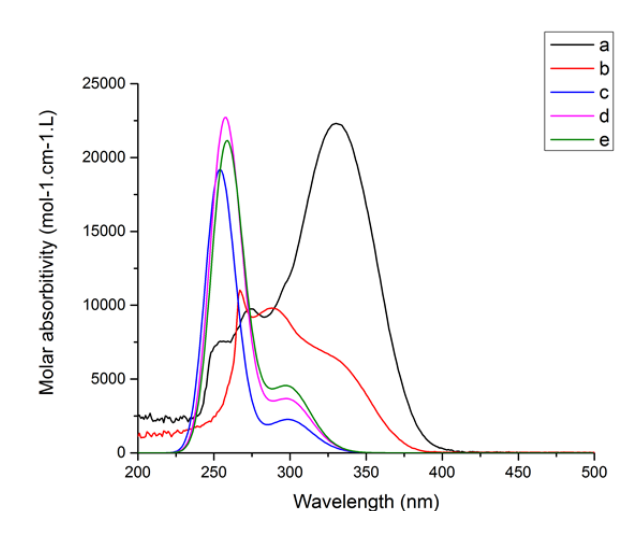


Figure 11. Electronic absorption spectra of compound 7; (a) experimental in Dioxane, (b) experimental in DMF, (c) theoretical in gas phase, (d) theoretical in Dioxane, (e) theoretical in DMF.

Unlike compound 3, the  $\pi$ -isoelectronic compound 7 is produced by switching F atom with OCH<sub>3</sub> group of compound 3. The experimental and theoretical electronic absorption spectra of compound 7 in Dioxane and DMF are shown in Fig. 11 and Table 9.

Table 9, Experimental and theoretical UV spectra of compound 7, calculated at TD-B3LYP/6-311G(d,p).

Ex. states	Theoretical													Experimental	
	Gas phase				Dioxane				DMF				Dioxane DMF		- Assig.
	Config.	Coeff.	f	λ, nm	Config.	Coeff.	f	λ, nm	Config.	Coeff.	f	λ, nm	$\lambda_{max}$ , nm	$\lambda_{max}$ , nm	
S1	84 -> 85	0.687	0.0519	301.9	84 -> 85	0.690	0.0903	300.8	83 -> 85 84 -> 85	0.108 0.688	0.1168	299.7	330.0	331.0	Electron delocal.
S2	84 -> 86	0.692	0.0176	286.4	84 -> 86	0.688	0.0243	281.4	84 -> 86	0.694	0.0015	281.9	274.0	288.0	CT-band
<b>S</b> 3	84 -> 87	0.697	0.0009	278.9	84 -> 87	0.693	0.0016	280.0	81 -> 85 84 -> 87	-0.123 0.688	0.0270	277.0			
S4	83 -> 85 84 -> 88	0.163 0.677	0.0032	262.4	83 -> 85 84 -> 88	-0.284 0.635	0.0256	261.7	83 -> 85 84 -> 88	-0.485 0.498	0.1323	261.0			
S5	83 -> 85 83 -> 86 84 -> 88	0.632 -0.179 -0.140	0.4241	254.7	83 -> 85 84 -> 85 84 -> 88	0.623 0.117 0.268	0.5743	257.7	83 -> 85 84 -> 85 84 -> 88	0.485 -0.136 0.471	0.4415	257.9	254.0	267.0	Electron delocal.
S6	80 -> 85 83 -> 85 83 -> 86	-0.257 0.189 0.603	0.1102	250.7	80 -> 85 83 -> 86	-0.261 0.629	0.0369	249.5	81 -> 85 83 -> 87	0.271 0.626	0.0156	246.9			

Observed spectra of compound 7 in Dioxane and DMF are composed of three bands appearing at 330, 274 and 254 nm for the former and 331, 288 and 267 nm for the latter. Changing of solvent polarity from Dioxane to DMF does not result in a significant change in wavelength for the first band, the second band is red shifted by 14 nm, while the third band is red shifted by 13 nm. The increase of solvent polarity results in a significant decrease in the intensity of the first band, the intensity of the second band remains unchanged, while the intensity of third band is increased. All bands are assigned to have  $\pi$ - $\pi$ \* character. Theoretical calculations is capable of assigning the observed UV Spectra of compound 7, which give excitations at 300.8 (S1), 281.4 (S2) and 257.7 (S5) nm in Dioxane. In DMF, the three bands reproduced at 299.7 (S1), 277.0 (S3) and 257.9 (S5) nm, while in gas phase the calculations give the bands at 301.9 (S1), 286.4 (S2) and 254.7 (S5) nm. All the observed transitions, theoretically calculated vertical excitations and their assignments are shown in Table 9. The orbitals,  $\Phi_{83}$ ,  $\Phi_{84}$ ,  $\Phi_{85}$ ,  $\Phi_{86}$  and  $\Phi_{87}$ , involved in the theoretical transitions of compound 7, are shown in Fig. 5v, 5w, 5x, 5y and 5z.

### Conclusion

Electronic structure of 5,7-diphenyl-4,7-dihydro-[1,2,4] triazolo [1,5-a] pyrimidine, compound 1 and its derivatives are investigated theoretically at B3LYP/6-311G(df,pd). The results indicate a satisfactory agreement between the theoretical calculations of vertical excitations computed at the TD-B3LYP/6-311G(d,p) and the experimental spectral observations as indicated by the quality of the theoretical UV spectra compared with the experimental one. All the studied compounds are found to be non-planar, where the dihedral angles results show that Ph-Y moiety is tilted by (36°-38°) and Ph-X moiety is out of the molecular plane by (49°-72°), resulting in a significant impact on the electronic and structural properties of compounds 1-7. The ground state properties of compounds 1-7 show that compound 2, which contains the nitro group, has the lowest  $E_{LUMO}$ , and  $E_g$  indicating highest reactivity, while compound 7 is found to have the highest polarity, as the computed dipole moments indicate. Electronic absorption spectra are investigated experimentally in Dioxane and DMF; and theoretically in gas phase, Dioxane and DMF using TD-B3LYP/6-311G(d,p). Band maxima ( $\lambda_{max}$ ) and intensities of the observed spectra are found to have solvent dependence. For compounds 1, 2, 4, 5 and 6, the first band shows a blue shift for compounds 1, 5, and 6 and a red shift for compound 2, while compound 4 shows solvent independence. The second band shows a red shift for compounds 1 and 4, while compounds 2, 5 and 6 show solvent independence. Compound 3 shows a slight blue shift for all bands, while in compound 7, the first band shows no solvent dependence, while the second and third bands show a red shift. The dissimilarity between the UV spectra of the  $\pi$ -isoelectronic compounds 3 and 7 may be attributed to the nature of the hyper conjugation between Ph-X, Ph-Y and the triazolo[1,5-a] pyrimidine fused ring (c. f. scheme 2). All the observed bands are assigned to be  $\pi$ - $\pi$ \* transitions as reflected from their intensities.

### References

- [1] Said, S. A., Amr, A. E., Sabry, N. M. and Abdalla, M. M. (2009). Analgesic, anticonvulsant and anti-inflammatory activities of some synthesized benzodiazipine, triazolopyrimidine and bis-imide derivatives. Eur. J. Med. Chem. 44(12): 4787-4792.
- [2] Rashad, A. E., Shamroukh, A. H., Hegab, M. I. and Awad, H. M. (2005). Synthesis of Some Biologically Active Pyrazoles and C-Nucleosides. ActaChim. Slov. 52: 429-434.
- [3] **Fischer**, **G.** (1993). 1,2,4-Triazolo [1,5-a] pyrimidines. Adv. Heter. Chem. 57: 81–138.
- [4] **Hafez, H. N. and El-Gazzar, A. B. A. (2009).** Synthesis and antitumor activity of substituted triazolo[4,3-a]pyrimidin-6-sulfonamide with an incorporated thiazolidinone moiety. Bioorg. Med. Chem. Lett. 19(15): 4143–4147.
- [5] Zhang, N., Ayral-Kaloustian, S., Nguyen, T., Afragola, J., Hernandez, R., Lucas, J., Gibbons, J. and Beyer, C. (2007). Synthesis and SAR of [1,2,4]Triazolo[1,5-a]pyrimidines, a Class of Anticancer Agents with a Unique Mechanism of Tubulin Inhibition. J. Med. Chem. 50(2): 319–327.
- [6] Havlicek, L., Fuksova, K., Krystof, V., Orsag, M., Vojtesek, B. and Strnad, M. (2005). 8-Azapurines as new inhibitors of cyclin-dependent kinases. Bioorg. Med. Chem. 13(18): 5399-5407.
- [7] Lakomska, I., Fandzloch, M., Muziol, T., Lis, T. and Jezierska, J. (2013). Synthesis, characterization and antitumor properties of two highly cytotoxic ruthenium (iii) complexes with bulky triazolopyrimidine ligands. Dalton Trans. 42(17): 6219-6226.
- [8] Kandeel, M. M., Mounir, A. A., Refaat, H. M. and Kassab, A. E. (2012). Synthesis of effective anticancer thieno [2,3-d] pyrimidine-4-ones and thieno [3,2-e]triazolo[4,3-c] pyrimidines. Int. J. Pharm. Pharm. Sci. 4(3): 438-448.
- [9] Salas, J. M., Quirós, M., Haj, M. A., Magán, R., Marín, C., Sáchez-Moreno, M. and Faure, R. (2001). Activity of Pt(II) and Ru(III) Triazolopyrimidine Complexes Against Parasites of the Genus Leishmania, Trypanosomas and Phytomonas. Met. Based Drugs. 8(3): 119–124.
- [10] Marwaha, A., White, J., El\_Mazouni, F., Creason, S. A., Kokkonda, S., Buckner, F. S., Charman, S. A., Phillips, M. A. and Rathod, P. K. (2012). Bioisosteric Transformations and Permutations in the Triazolopyrimidine Scaffold To Identify the Minimum Pharmacophore Required for Inhibitory Activity against Plasmodium falciparum Dihydroorotate Dehydrogenase. J. Med. Chem. 55(17): 7425–7436.

- [11] **Zhang, N., Ayral-Kaloustian, S., Nguyen, T., Hernandez, R., Beyer, C.** (2007). 2-Cyanoaminopyrimidines as a class of antitumor agents that promote tubulin polymerization. Bioorg. Med. Chem. Lett. 17(11): 3003-3005.
- [12] Beyer, C. F., Zhang, N., Hernandez, R., Vitale, D., Lucas, J., Nguyen, T., Discafani, C., Ayral-Kaloustian, S. and Gibbons, J. J. (2008). TTI-237: A Novel Microtubule-Active Compound with In vivo Antitumor Activity. Cancer Res. 68(7): 2292-2300.
- [13] Yu, B., Shi, X., Zheng, Y., Fang, Y., Zhang, E., Yu, D. and Liu, H. (2013). A novel [1,2,4] triazolo [1,5-a] pyrimidine-based phenyl-linked steroid dimer: Synthesis and its cytotoxic activity. Eur. J. Med. Chem. 69: 323-330.
- [14] **Ghorab, M. M., El-gazzar, M. G. and Alsaid, M. S. (2014).** Design and synthesis of novel thiophenes bearing biologically active aniline, aminopyridine, benzylamine, nicotinamide, pyrimidine and triazolopyrimidine moieties searching for cytotoxic agents. ActaPolon. Pharm.-Drug Res. 71(3): 401-407.
- [15] **El-Gendy, M. M. A., Shaaban, M., Shaaban, K. A., El-Bondkly, A. M. and Laatsch, H. (2008).** Essramycin: A First Triazolopyrimidine Antibiotic Isolated from Nature. J. Antibiot. 61(3): 149–157.
- [16] **Parameswari, K., Chitra, S., Kavitha, S., Rajpriya, J. and Selvaraj, A (2011).** Adsorption and Inhibitive Properties of Triazolo-pyrimidine Derivatives in Acid Corrosion of Mild Steel. E-Journal of Chemistry. 8(3): 1250-1257.
- [17] **Zhou, L., Ismaili, J., Stordeur, P., Thielemans, K., Goldman, M. and Pradier, O. (1999).** Inhibition of the CD40 Pathway of Monocyte Activation by Triazolopyrimidine. Clin. Imm. 93(3): 232–238.
- [18] Chen, Q., Zhu, X., Jiang, L., Liu, Z. and Yang, G. (2008). Synthesis, antifungal activity and CoMFA analysis of novel 1,2,4-triazolo[1,5-a]pyrimidine derivatives. Eur. J. Med. Chem. 43(3): 595-603.
- [19] Uryu, S., Tokuhiro, S., Murasugi, T. and Oda, T. (2002). A novel compound, RS-1178, specifically inhibits neuronal cell death mediated by  $\beta$ -amyloid-induced macrophage activation in vitro. Brain Res. 946(2): 298-306.
- [20] Li, H., Tatlock, J., Linton, A., Gonzalez, J., Jewell, T., Patel, L., Ludlum, S., Drowns, M., Rahavendran, S. V., Skor, H., Hunter, R., Shi, S. T., Herlihy, K. J., Parge, H., Hickey, M., Yu, X., Chau, F., Nonomiya, J. and Lewis, C. (2009). Discovery of (R)-6-Cyclopentyl-6-(2-(2,6-diethylpyridin-4-yl)ethyl)-3-((5,7-dimethyl-[1,2,4] triazolo [1,5-a] pyrimidin-2-yl)methyl)-4-hydroxy-5,6-dihydropyran-2-one (PF-00868554) as a Potent and Orally Available Hepatitis C Virus Polymerase Inhibitor. J. Med. Chem. 52(5): 1255–1258.
- [21] Chen, C., Lv, L., Ji, F., Chen, Q., Xu, H., Niu, C., Xi, Z. and Yang, G. (2009). Design and synthesis of N-2,6-difluorophenyl-5-methoxyl-1,2,4-triazolo[1,5-a]-pyrimidine-2-sulfonamide as acetohydroxyacid synthase inhibitor. Bioorg. Med. Chem. 17(8): 3011-3017.
- [22] Caballero, A. B., Rodríguez-Diéguez, A., Quirós, M., Salas, J. M., Huertas, Ó.,Ramírez-Macías, I., Olmo, F., Marín, C., Chaves-Lemaur, G., Gutierrez-Sánchez, R. and Sánchez-Moreno, M. (2014). Triazolopyrimidine compounds containing first-row transition metals and their activity against the neglected infectious Chagas disease and leishmaniasis. Eur. J. Med. Chem. 85: 526–534.
- [23] Kumar, R., Nair, R. R., Dhiman, S. S., Sharma, J. and Prakash, O. (2009). Organoiodine (III)-mediated synthesis of 3-aryl/heteroaryl-5,7-dimethyl-1,2,4-triazolo[4,3-c]pyrimidines as antibacterial agents. Eur. J. Med. Chem. 44(5): 2260-2264.
- [24] **Abdel-Rahman, H. M., El-Koussi, N. A. and Hassan, H. Y. (2009).** Fluorinated 1,2,4-Triazolo[1,5-a]pyrimidine-6-carboxylic Acid Derivatives as Antimycobacterial Agents. Arch. Pharm. Weinheim. 342(2): 94–99.
- [25] Girasolo, M. A., Canfora, L., Sabatino, P., Schillaci, D., Foresti, E., Rubino, S., Ruisi, G. and Stocco, G. (2012). Synthesis, characterization, crystal structures and in vitro antistaphylococcal activity of organotin(IV) derivatives with 5,7-disubstituted-1,2,4-triazolo[1,5-a]pyrimidine. J. Inorg. Biochem. 106(1): 156–163.
- [26] Peng, H., Kumaravel, G., Yao, G., Sha, L., Wang, J., Van Vlijmen, H., Bohnert, T., Huang, C., Vu, C. B., Ensinger, C. L., Chang, H., Engber, T. M., Whalley, E. T. and Petter, R. C. (2004). Novel bicyclic piperazine derivatives of triazolotriazine and triazolopyrimidines as highly potent and selective adenosine A2A receptor antagonists. J. Med. Chem. 47(25): 6218–6229.
- [27] Vu, C. B., Shields, P., Peng, B., Kumaravel, G., Jin, X., Phadke, D., Wang, J., Engber, T., Ayyub, E. and Petter, R. C. (2004). Triamino derivatives of triazolotriazine and triazolopyrimidine as adenosine A<sub>2a</sub> receptor antagonists. Bioorg. Med. Chem. Lett. 14(19): 4835–4838.

- [28] Ram, V. J., Pratibha, S., Singh, S. K., Kandpal, M. and Tekwani, B. L. (1997). Functionalized azoles and triazolo[1,5-a]pyrimidines as latent leishmanicides. Bioorg. Med. Chem. Lett. 7(8): 1087–1090.
- [29] **Ojha, P. K. and Roy, K. (2010).**Chemometric modeling, docking and in silico design of triazolopyrimidine-based dihydroorotate dehydrogenase inhibitors as antimalarials. Eur. J. Med. Chem. 45(10): 4645–4656.
- [30] Okamura, T., Kurogi, Y., Hashimoto, K., Nishikawa, H. and Nagao, Y. (2004). Facile synthesis of fused 1,2,4-triazolo[1,5-c]pyrimidine derivatives as human adenosine A3 receptor ligands. Bioorg. Med. Chem. Lett. 14(10): 2443–2446.
- [31] **Novinson, T., Springer, R. H., O'Brien, D. E., Scholten, M. B., Miller, J. P. and Robins, R. K. (1982).** 2-(Alkylthio)-1,2,4-triazolo[1,5-a]pyrimidines as adenosine 3',5'-monophosphate phosphodiesterase inhibitors with potential as new cardiovascular agents. J. Med. Chem. 25(4): 420–426.
- [32] Kleschick, W. A., Costales, M. J., Dunbar, J. E., Meiklel, R. W., Monte, W. T., Pearson, N. R., Snider, S. W., Vinogradoff, A. P. (1990). New herbicidal derivatives of 1,2,4-triazolo [1,5-a] pyrimidine. Pestic. Sci. 29(3): 341–355.
- [33] Moustafa, H., Shibl, M. F., Hilal, R., Ali, L. I. and Abdel Halim, S. (2011). Electronic Absorption Spectra of Some Triazolopyrimidine Derivatives. Int. J. Spec. vol. 2011: Article ID 394948 8 pages, doi:10.1155/2011/394948 (http://dx.doi.org/10.1155/2011/394948).
- [34] Moxon, G.H. and Slifkin, M.A. (1972). Solvent effects on the electronic spectra of certain heterocyclic molecules. Spec. Acta A: Mol. Spec. 28(12): 2419–2432.
- [35] Caballero, A. B., Rodríguez-Diéguez, A., Quirós, M., Lezama, L. and Salas, J. M. (2011). New copper(II), nickel(II) and zinc(II) complexes with 1,2,4-triazolo[1,5-a]pyrimidines and the chelating ligand 1,3-propanediamine: An unexpected coordination behavior for the 7-amine-derivative. Inorg. Chim. Acta. 378(1): 194–201.
- [36] Malecki, J.G. and Kruszynski, R. (2010). Synthesis, spectroscopic and structural characterization of new complex of ruthenium(II) with Hmtpo ligand. Polyhedron. 29(3): 1023–1028.
- [37] **Dobado, J. A., Grigoleit, S. and Molina, J. M. (2000).** Theoretical characterization of 5-oxo, 7-oxo and 5-oxo-7-amino[1,2,4]triazolo[1,5-a]pyrimidines. J. Chem. Soc., Perkin Trans. 2. 8: 1675-1680.
- [38] **Hassaneen, H. M. E. and Farghaly, T. A.** (2014). A simple, convenient, One-Pot Synthesis of Dihydro-azolopyrimidines, DFT calculation, and NMR Determination by using H-Ferrierite Zeolite as Catalyst. J. heterocyclic Chemistry. doi: 10.1002/jhet.2152 (http://dx.doi.org/10.1002/jhet.2152).
- [39] **Becke, A. D.** (1993). Density-functional thermochemistry. III. The role of exact exchange. J. Chem. Phys., 98(7): 5648-5652.
- [40] Lee, C., Yang, W. and Parr, R. G. (1998). Development of the Colle-Salvetti correlation-energy formula into a functional of the electron density. Phys. Rev. B. 37(2): 785-789.
- [41] **M. E. Casida** (1996). Time-dependent density functional response theory of molecular systems: theory, computational methods, and functionals. In J. Seminario (Ed.), Recent Developments and Applications of Modern Density Functional Theory, Elsevier, Amsterdam. pp. 391 439.
- [42] **Miertuš, S., Scrocco, E. and Tomasi, J. (1981).** Electrostatic interaction of a solute with a continuum. A direct utilizaion of AB initio molecular potentials for the prevision of solvent effects. Chem. Phys. 55(1): 117-129.
- [43] **Pascual-ahuir**, **J. L.**, **Silla**, **E. and Tuñon**, **I.** (1994). GEPOL: An improved description of molecular surfaces. III. A new algorithm for the computation of a solvent-excluding surface. J. Comp. Chem. 15(10): 1127–1138.
- [44] Frisch, M. J., Trucks, G. W., Schlegel, H. B., Scuseria, G. E., Robb, M. A., Cheeseman, J. R., Scalmani, Barone, G., Mennucci, V. B., Petersson, G. A., Nakatsuji, H., Caricato, M., Li, X., Hratchian, H. P., Izmaylov, A. F., Bloino, J., Zheng, G., Sonnenberg, J. L., Hada, M., Ehara, M., Toyota, K., Fukuda, R., Hasegawa, J., Ishida, M., Nakajima, T., Honda, Y., Kitao, O., Nakai, H., Vreven, T., Montgomery, J. A., Jr., Peralta, J. E., Ogliaro, F., Bearpark, M., Heyd, J. J., Brothers, E., Kudin, K. N., Staroverov, V. N., Kobayashi, R., Normand, J., Raghavachari, K., Rendell, A., Burant, J. C., Iyengar, S. S., Tomasi, J., Cossi, M., Rega, N., Millam, J. M., Klene, M., Knox, J. E., Cross, J. B., Bakken, V., Adamo, C., Jaramillo, J., Gomperts, R., Stratmann, R. E., Yazyev, O., Austin, A. J., Cammi, R., Pomelli, C., Ochterski, J. W., Martin, R. L.,

Morokuma, K., Zakrzewski, V. G., Voth, G. A., Salvador, P., Dannenberg, J. J., Dapprich, S., Daniels, A. D., Farkas, O., Foresman, J. B., Ortiz, J. V., Cioslowski, J. and Fox, D. J. (2009). Gaussian 09, Revision A. I., Gaussian, Inc., Wallingford CT.